ELSEVIER

Journal of Chromatography A, 943 (2001) 63–75

JOURNAL OF CHROMATOGRAPHY A

www.elsevier.com/locate/chroma

Nd–Fe–B alloy-densified agarose gel for expanded bed adsorption of proteins

Xiao–Dong Tong, Yan Sun*

Department of Biochemical Engineering, School of Chemical Engineering and Technology, Tianjin University, Tianjin 300072, China

Received 27 June 2001; received in revised form 18 October 2001; accepted 24 October 2001

Abstract

Novel dense composite adsorbents for expanded bed adsorption of protein have been fabricated by coating 4% agarose gel onto Nd–Fe–B alloy powder by a water-in-oil emulsification method. Two composite matrices, namely Nd–Fe–B alloy-densified agarose (NFBA) gels with different size distributions and densities, NFBA-S (50–165 μm, 1.88 g/ml) and NFBA-L (140–300 μm, 2.04 g/ml), were produced. Lysozyme was used as a model protein to test the adsorption capacity and kinetics for the NFBA gels modified by Cibacron blue 3GA (CB-NFBA gels). Liquid-phase dispersion behavior in the expanded beds was examined by measurements of residence time distributions, and compared with that of Streamline SP (Amersham–Pharmacia Biotech, Sweden). The dependence of axial mixing in the expanded beds on flow velocity, bed expansion degree, settled bed height, and viscosity of liquid phase was investigated. Breakthrough curves of lysozyme in the expanded beds of the CB-NFBA gels were also examined. The dynamic binding capacity at 5% breakthrough was 23.3 mg/ml matrix for the CB-NFBA-S gels, and 16.7 mg/ml matrix for the CB-NFBA-L, at a flow velocity of 220 cm/h. The results indicate that the NFBA gels are promising for expanded bed adsorption of proteins.

Keywords: Adsorption; Expanded bed chromatography; Agarose gels; Nd–Fe–B alloys; Stationary phases, LC; Fluidised bed; Proteins; Lysozyme

1. Introduction

The expanded bed is a low back-mixing liquid fluidized bed achieved by a special design of the column and solid matrix with a defined size and/or density distribution. As an innovative chromatography mode, expanded bed adsorption provides an increased bed voidage with increasing flow velocity. The larger interparticle void fraction makes it possible for crude feedstock containing particulate materials such as cells, cell debris and other possible fine particles to pass through. Therefore, expanded bed adsorption can be used for the primary recovery of desired product directly from unclarified feedstocks, benefiting in the reduction of the number of separation steps in a downstream bioprocess [1–3]. A number of publications have demonstrated the concept of expanded bed adsorption and various applications of expanded bed to target product recovery [4–7].

As the key element of expanded bed adsorption, synthesis of suitable solid matrices has greatly

*Corresponding author. Tel.: +86-22-2740; 6590; fax: +86-22-2740-6590.

E-mail address: ysun@tju.edu.cn (Y. Sun).

0021-9673/02/$ – see front matter
PII: S0021-9673(01)01435-2

attracted the attention of researchers during recent years [8,9]. The basic criteria for the matrices suitable for expanded bed adsorption are formulated as being a sufficient density of the material and a distribution of particle size [10]. The higher density matrix is needed for the stable operation at higher flow velocity, and the appropriate size distribution contributes significantly to reducing the mixing in the column. The adsorption capacity and mass transfer characteristics should also be considered in the synthesis of matrices to ensure bed efficiency [9].

At present, there are primarily two ways to obtain matrices for expanded bed adsorption. A simple way is to use high-density porous materials, such as cellulose bead [8], silica gel [11], and zirconium oxide particles [12,13]. The other strategy involves the use of high-density materials as the internal cores to weigh the solid phase. Commercially available matrices, such as cross-linked agarose weighed by incorporating fine crystalline quartz or metal particles, marked under the trade name Streamline, have been widely used [1,2,5–7]. These matrices normally have densities of 1.1–1.3 g/ml and sizes of 80–300 μm [2]. Since crude feedstocks such as cell disruptates could be quite viscous, the small density differences between the crude feedstocks and the solid phases would limit their application to expanded bed adsorption. Therefore, even heavier and larger solid materials, such as nickel powder, stainless steel spheres, titanium oxide, zirconium oxide and hafnium oxide, have been used as the core to provide alternative solid phases for expanded bed adsorption [9,14–16].

In this work, we chose Nd–Fe–B alloy powder to prepare a high-density gel. Nd–Fe–B alloy powder offers the possibility of higher density (7.4 g/ml) as the core, than the classical solid materials, and is remarkably stable to strong cleaning agents (i.e., sodium hydroxide), and permits repeated cleaning-in-place cycles. Additionally, Nd–Fe–B alloy powder exhibits magnetic properties, and can be rapidly separated in a magnetic field. Thus, Nd–Fe–B alloy powder could also been utilized to prepare adsorbents for both expanded bed adsorption and magnetically stabilized fluidized bed (MSFB). This article describes the use of a water-in-oil emulsification technique [9] for the preparation of high-density agarose gels incorporating Nd–Fe–B alloy powder. The densified gels, after modification with Cibacron blue 3GA, were characterized with respect to protein adsorption equilibrium, kinetics, and flow hydrodynamics in expanded bed operation. The breakthrough curves of lysozyme in the expanded beds were also investigated. Comparisons of the matrices with Streamline SP in terms of flow hydrodynamics, and with Cibacron blue 3GA modified Streamline for static and dynamic adsorption performances, are discussed.

2. Materials and methods

2.1. Materials

Low gelling temperature agarose (A4018), lysozyme and Cibacron blue 3GA (CB) were purchased from Sigma (St. Louis, MO, USA). Nd–Fe–B alloy powder was a gift from SanHuan Lucky New Materials (Tianjin, China). The alloy powder consisted of 15% Nd, 77% Fe and 8% B, with a mean density of 7.4 g/ml and a size distribution of 17–80 μm. Sorbitan monooleate (Span 80) was obtained from Tianhai Fine Chemicals (Tianjin, China). Streamline SP and Streamline quartz base matrix were provided by Amersham–Pharmacia Biotech (Uppsala, Sweden). Permanent magnets (maximum field strength, 0.402 Tesla) were provided by the Research Institute of Rare Earth Elements (Baotou, China). Glycerol was obtained from Tianjin Letai Chemical Company (Tianjin, China). Edible soybean oil was purchased from a local store. All other chemicals were of analytical grade from local sources.

2.2. Preparation of the Nd–Fe–B alloy-densified agarose gel

Prior to being used, the Nd–Fe–B alloy powder was pretreated using the following procedure [14]. Thirty grams of the powder were cleaned by washing with distilled water and ethanol to remove any fouling. Then the powder was dipped in 50 ml of 3 mol/l NaOH to oxidize the surface for 10 min. Finally, the powder was rinsed with distilled water and dried.

The Nd–Fe–B alloy-densified agarose gel was

prepared by a method similar to that of Pålsson et al. [9], but reaction temperature, reaction time, and the volume ratio of liquid to solid phases were adjusted due to the difference in the solid-phase properties. The preparation procedure is as follows. A 1000-ml round-bottomed glass flask, equipped with a half-moon paddle fitting to the flask bottom for agitation, was used for the water–oil emulsification experiments to prepare the Nd–Fe–B alloy-densified agarose gel. It was filled with 600 ml of the soybean oil containing 10 g/l Span 80, and the oil phase was heated to 90°C in a water bath. The paddle was adjusted as near as possible to the flask bottom for the agitation of the dense particles. Agarose solution (60 ml; 4%, w/v) was prepared by heating to 90°C in a water bath, and 30 g of the Nd–Fe–B alloy particles were added to the solution under agitation and ultrasonication. Then the liquid–solid mixture was slowly poured into the oil phase. After agitation at 1400 rpm for 30 min, tap water was supplied to cool the suspension to 15°C. After stirring at 15°C for 30 min, the densified gels were recovered by the permanent magnet from the oil phase. The particles were then washed thoroughly with acetone to remove any adsorbed oil, and then were rinsed with distilled water.

2.3. Crosslinking and CB coupling

The NFBA gel was mixed with the same volume of 1.0 mol/l NaOH containing 5 g/l sodium borohydride. After agitation at 150 rpm for 30 min, epichlorohydrin was introduced to a final concentration of 2% (v/v). The reaction was carried out at 25°C for 4 h. Then, the cross-linked particles were washed thoroughly with distilled water, and reduced with the same volume of 2.0 mol/l NaOH containing 5 g/l sodium borohydride by boiling for 2 min.

After cross-linking, the NFBA gel was screened with 54-, 125- and 300-μm standard sieves, and two fractions with different size distributions were obtained. The fraction with the larger size (140–300 μm) is denoted as NFBA-L, and that with the smaller size (50–165 μm) as NFBA-S. A small fraction of the particles (<5%) passed through the 54-μm standard sieve; this was mostly non-coated Nd–Fe–B powder as observed by microscopy. Only a little non-coated Nd–Fe–B powder was found in the retained fractions.

The cross-linked gels were modified with CB as described by He et al. [17]. For CB coupling density determination, around 0.2 ml of the drained particles was digested in 10 ml of 0.1 mol/l HCl solution at 80°C. The same amount of unmodified particles was used as a reference. After adjustment to pH 2.0 by titration with 0.1 mol/l NaOH, CB concentration in the solution was measured, and the coupling density of CB was determined. The Streamline base matrix was modified with CB by the same procedure.

2.4. Protein adsorption

Lysozyme was used as a model protein to test the adsorption characteristics of the NFBA gels modified by CB (CB-NFBA) and Streamline modified by CB (CB-Streamline). In adsorption equilibrium experiments, 0.1 ml of the drained adsorbents was added to 10 ml of lysozyme solution of different concentrations. The aqueous solution was 0.01 mol/l Tris–HCl buffer (pH 7.6). Adsorption experiments were conducted at 25°C for 6 h in a shaking incubator. At the end of adsorption, the solid-phase was magnetically separated, and the supernatant was analyzed for protein concentration. The adsorbed mass of protein was calculated by from the mass balance.

In kinetic experiments, 0.5 ml of the drained gel was mixed with 50 ml of 0.5 mg/ml lysozyme solution in 0.01 mol/l Tris–HCl buffer (pH 7.6). The adsorption was carried out in the shaking incubator at 25°C. Every few minutes, about 2 ml of the liquid phase was aspirated using a suction tube to determine protein concentration, and the sample was returned to the vessel immediately. This procedure took less than 20 s. Using this procedure, the time course of lysozyme concentration decrease was determined.

2.5. Expanded bed operation

A glass column (70 cm×9.5 mm I.D.) with a stainless steel mesh (with 54-μm openings) as the liquid distributor and a prolonged top adapter was used for expanded bed experiments. The top adapter was positioned 2.0±0.2 cm above the bed surface. A Series IV piston pump (Scientific Systems, USA)

was employed for liquid-phase supply. The column was connected to a manual injection valve (model GJ-605F, Dalian Institute of Physics and Chemistry, Dalian, China) with a 200-μl sample loop. The outlet signal was monitored with a UV detector at 280 nm. The column outlet and the UV detector were linked with 2.0-mm I.D. silicon rubber tubing. The other devices were connected using 1.0-mm I.D. plastic tubing. The UV detector was placed as near as possible to the column outlet to reduce the dead volume in the experimental system. Proper column vertical alignment was confirmed in all experiments.

Distilled water and a 10% (v/v) glycerol solution were used as the liquid phases for expanded bed experiments. Most experiments of bed expansion and flow hydrodynamics were performed at 20°C with a settled bed height of 7.2 or 15.0±0.2 cm. Liquid dispersion behavior in the expanded bed was determined by residence time distribution (RTD) experiments. In the RTD experiments, 200 μl of 25% (v/v) acetone solution were injected as the tracer solution at the bottom inlet of the column, and the output signal at the column outlet was acquired by a personal computer equipped with a data acquisition system. Individual experiments were performed for the complete experimental rig in the presence or absence of adsorbent in order to identify the contribution of the volume of fittings and the 2.0-cm zone above the bed surface.

Moment analyses of the RTD data showed the mean residence time and the variance for the expanded bed. Considering the expanded bed as an open vessel, the Bodenstein number, Bo, can be calculated from the following formula [18]:

$$\sigma_\theta^2 = \frac{2}{\mathrm{Bo}} + \frac{8}{\mathrm{Bo}^2} \quad (1)$$

The Bodenstein number relates the ratio of convective to dispersion mass transport, defined as:

$$\mathrm{Bo} = \frac{UH}{\varepsilon D_{\mathrm{ax}}} \quad (2)$$

Thus, the axial mixing coefficient D_{ax}, can be calculated from Eq. (2).

2.6. Dynamic adsorption of lysozyme by expanded beds

The breakthrough behavior of lysozyme in the expanded beds of the CB-NFBA gels and CB-Streamline was investigated by frontal adsorption experiments. All experiments were carried out at 25°C with a settled bed height of 5.0±0.2 cm. Lysozyme solution (0.5 mg/ml) in 0.01 mol/l Tris–HCl was used. Before applying lysozyme solution, the bed was allowed to expand stably at least 30 min with Tris–HCl buffer, and the flow hydrodynamics of the beds was determined initially. A superficial velocity of 220 cm/h was necessary for the CB-Streamline bed to expand 2-fold. Thus, two operation modes for the CB-NFBA-S and CB-NFBA-L beds were used for comparison with the CB-Streamline bed: one was at 2-fold bed expansion, and the other was at a superficial velocity of 220 cm/h.

Dynamic binding capacity (DBC) was calculated from lysozyme breakthrough curves. The total amount of lysozyme adsorbed at 5% breakthrough point was calculated using the method of Griffith et al. [13]:

$$Q_{5\%} = U \cdot c_0 \int_0^{t(c/c_0=0.05)} \left(1 - \frac{c}{c_0}\right) \mathrm{d}t \quad (3)$$

The DBC is defined as the total amount of lysozyme adsorbed in the column, subtracting the lysozyme in the dead spaces per unit adsorbent volume. The amount of lysozyme in dead spaces was calculated by

$$Q_{\mathrm{d}} = V_{\mathrm{d}} \cdot c_0 \quad (4)$$

Thus,

$$\mathrm{DBC} = \frac{Q_{5\%} - Q_{\mathrm{d}}}{V_{\mathrm{S}}} \quad (5)$$

2.7. Analysis and measurements

CB concentration was measured using a spectrophotometer at 620 nm with a molar extinction coefficient of 1.03×10^4 l mol^{-1} cm^{-1} at pH 2.0, which was determined by preliminary experiment. BSA concentration was determined by the Bradford method [19]. In breakthrough experiments, the protein content in the effluent was measured using a flow UV monitor at 280 nm, and was analyzed additionally every 10 min using the Bradford method.

The morphology of the NFBA gel was observed

using a model XS-18 optical microscope (Jiangnan Scientific Instruments, China), and the image was recorded using a Model YT-310B CCD (charge coupled device) camera. The size distribution of the particles was measured with a Mastersizer 2000 unit (Malvern Instruments, Malvern, UK). Solid densities were measured using a pycnometer at 20°C.

3. Results and discussion

3.1. Characterization of the NFBA gels

Fig. 1 shows the micrographs of the NFBA-S and NFBA-L matrices. It can be seen that the NFBA-S is composed of a few single particles of Nd–Fe–B alloy powder (the black dots) entrapped in the agarose gel (the transparent area), while the NFBA-L consists of an agglomerate of the Nd–Fe–B powder. The NFBA gels showed strong magnetic responsiveness, and could be quickly recovered in magnetic separations. Moreover, we observed no obvious aggregation of the NFBA gels under microscopy after the matrices had been treated in a magnetic field. The NFBA gels were stored at 4°C with 20% ethanol until further treatment. The NFBA gels showed no visible changes after a storage of longer than 3 months. Furthermore, no change of appearance after recycled use was observed in the cross-linked NFBA gels. This indicates the stability of the dense matrices.

The particle size distributions of the NFBA gels are shown in Fig. 2. The volumetric diameters d_{10} and d_{90} are defined as the points on the size distribution where, respectively, 10 and 90% (v/v) of the particles are smaller than the stated diameter. It can be seen from the statistics of the size distributions that 80% (v/v) are in the range of 50–165 μm for the NFBA-S gels, and 140–300 μm for the NFBA-L gels. The physical properties of Nd–Fe–B alloy powder and the composite agarose gels are listed in Table 1. In the table, agarose gel volume fraction in the composite matrices (f) is calculated from the following equation derived from mass balance:

$$f = \frac{\rho_C - \rho_P}{\rho_C - \rho_A} \quad (6)$$

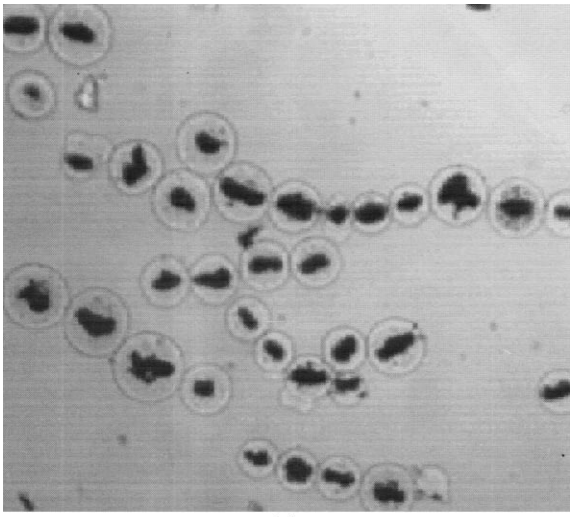
(a)

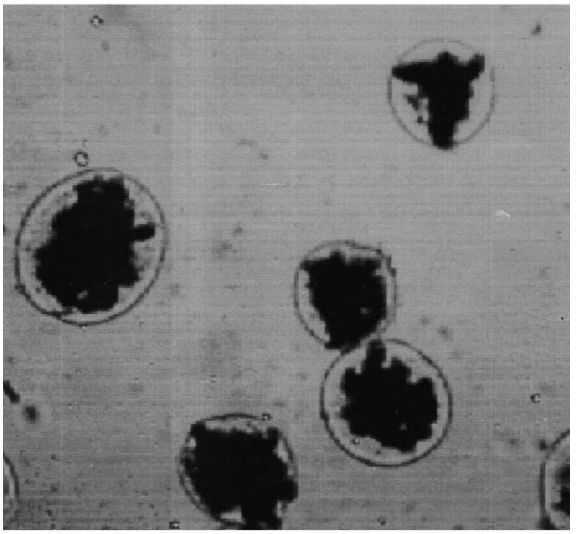
(b)

Fig. 1. Photographs of (a) NFBA-S and (b) NFBA-L particles taken with a CCD camera through an optical microscope (×160).

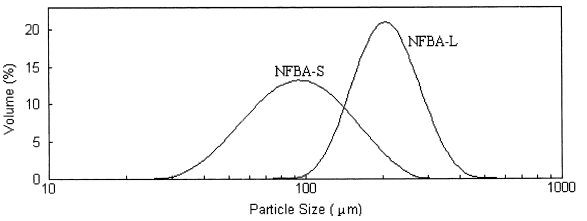

Fig. 2. Particle size distribution of the NFBA gels measured with the Malvern 2000 unit.

Table 1
Physical properties of Nd–Fe–B alloy powder and NFBA gels

Matrix	Size range (μm)	Mean size[a] (μm)	ρ_s (g/ml)	f
Nd–Fe–B powder	17–80	43	7.40	0
NFBA-S	50–165	102	1.88	0.87
NFBA-L	140–300	215	2.04	0.84

[a] The volume-weighted mean diameter of the matrices.

It is found that the densities of the NFBA matrices lie in the range around 2 g/ml, and the NFBA-L is heavier than the NFBA-S because the former consists of more alloy powder. For the same reason, the f value of NFBA-L is smaller than that of NFBA-S. Moreover, the densities of the composite matrices are much higher than those of the commercially available Streamline materials [2] and silica gels [16], and slightly smaller than those of the reported composite matrices, such as stainless steel agarose beads [9], zirconium oxide [13], and titanium oxide [16].

Fig. 3 shows the adsorption isotherms of lysozyme to the dye–ligand composite adsorbents and CB-Streamline. The adsorption isotherms were well expressed by the Langmuir equation:

$$q = \frac{q_m c}{K_d + c} \quad (7)$$

The adsorption capacity of lysozyme to the CB-NFBA-S gels was as high as 78.5 mg/ml, similar to that to the CB-Streamline, with approximately the same level of CB coupling density (Table 2). It is found that the capacity of the CB-NFBA-L gels was lower than that of the CB-NFBA-S gels. This is considered to be due to its lower CB coupling density (Table 2). The decrease of protein adsorption capacity to dye–ligand adsorbents with decreasing CB coupling density has been well recognized [20,21].

Intraparticle diffusion of lysozyme to the CB-NFBA gels and CB-Streamline was estimated using the pore diffusion model incorporating the external film mass transfer [22]. The pore diffusion coefficients thus obtained are provided in Table 2. It can be seen that the pore diffusion coefficients of lysozyme to the three adsorbents are $2.0–3.8\times10^{-11}$ m^2/s, which are nearly the same as that of lysozyme diffusion to Streamline SP (3.5×10^{-11} m^2/s) [23].

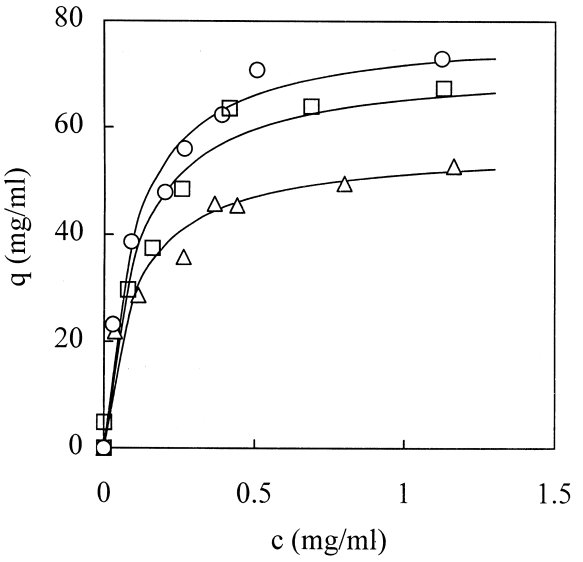

Fig. 3. Adsorption isotherms of lysozyme to (○) CB-NFBA-S, (△) CB-NFBA-L and (□) Streamline CB. Solid lines are calculated from the Langmuir equation.

3.2. Bed expansion characteristics

Lali et al. [24] claimed that the wall effect on bed expansion behavior is negligible as long as the ratio of column to particle diameter is larger than 20. Because the value of this ratio in the present work was larger than 40, the bed expansion behavior in the experiments should not be influenced by the wall effect. The bed expansions for the dense composite matrices are shown in Fig. 4. For comparison, the bed expansion characteristics of Streamline SP are

Table 2
Parameters in the Langmuir equation and pore diffusion coefficients for the three adsorbents

Matrix	CB (μmol/ml)	q_m (mg/ml)	K_d (mg/ml)	D_p (10^{-11} m^2/s)
NFBA-S	6.9	78.5	0.095	2.0
NFBA-L	5.5	56.2	0.097	2.6
CB-Streamline	6.7	71.8	0.102	3.9

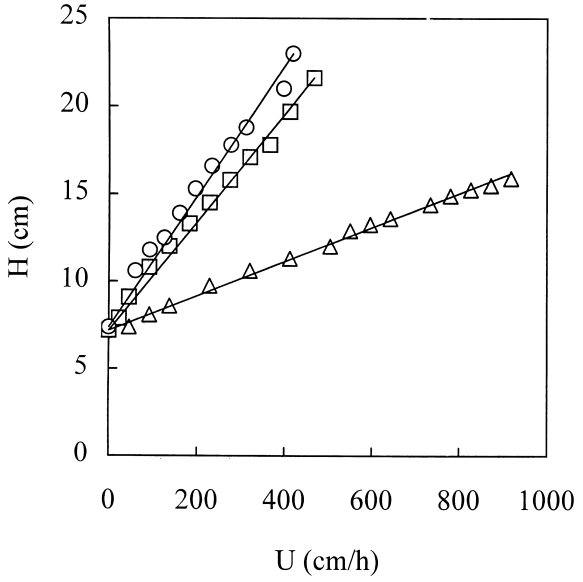

Fig. 4. Bed expansion behavior of various matrices: (○) NFBA-S, (△) NFBA-L and (□) Streamline SP. Settled bed height was 7.2±0.2 cm.

also provided. The Richardson–Zaki equation was carried out to estimate the variation of the bed expansion as a function of flow velocity through the bed [25]:

$$U = U_t \varepsilon^n \tag{8}$$

The average bed voidage can be estimated from the following formula [26]:

$$\varepsilon = 1 - (1 - \varepsilon_0) \cdot \frac{H_0}{H} \tag{9}$$

The packed-bed voidage, ε_0, was measured in 10-ml measuring cylinder. It was determined to be 0.36 for the NFBA-S, and 0.41 for the NFBA-L. The packed-bed voidage for Streamline SP was reported to be 0.4 [27]. Using these data, the values of n and U_t in Eq. (8) were estimated. Table 3 lists the results. It is found that the values of n are in the range of 5.4–5.9, reasonably close to the theoretical value of 4.8 in the laminar flow regime [25,27].

Table 3 also provides the terminal velocity determined by the Stokes' equation:

Table 3
Richardson–Zaki parameters and comparison between the experimental and theoretical terminal velocities

Matrix	n	U_t (mm/s)	
		Expt.	Stokes' equation
NFBA-S	5.39	4.18	4.97
NFBA-L	5.87	14.3	26.1
Streamline SP[a]	5.42	4.38	4.17

[a] The mean particle size and density of Streamline SP at 20°C were measured to be 195 μm and 1.2 g/ml, respectively.

$$U_t = \frac{d_p^2(\rho_s - \rho)g}{18\mu} \tag{10}$$

A comparison of the experimentally determined terminal velocities for the NFBA-S and NFBA-L from Eq. (8) to the values calculated from the Stokes' equation reveals a significant difference. For example, the experimentally determined value for the NFBA-L was only about a half that from the Stokes' equation. In contrast, the experimental and the theoretical terminal velocities for Streamline SP were nearly the same. The discrepancy between these results is comparable to those reported in the literature. For example, Thömmes et al. [1] found that the terminal velocity calculated by the Stokes' equation was about an order higher than that experimentally determined in the fluidized bed of controlled pore glass. They explained the observation as the porous nature and very irregular shape of the glass matrix. However, an opposite tendency was observed by Chang and Chase [27] with Streamline-based adsorbents when viscous liquid phases were employed. Karau et al. [28] considered that the groupwise motion of particles due to the interaction of viscous drag led to the difference between experimentally determined and theoretically calculated terminal velocities. In the present work, the dense composite NFBA matrices would have a large density distribution due to the uneven allocation of the alloy material in the agarose beads. This would result in the smaller experimental terminal velocity than that calculated from the Stokes' theory with a mean particle density. As shown in Fig. 4, to reach a 2-fold bed expansion, the flow velocity needed was 182

cm/h for the NFBA-S, 735 cm/h for the NFBA-L, and 230 cm/h for Streamline SP.

3.3. Axial dispersion behavior in the expanded beds

The efficiency of an expanded bed adsorption is closely related to the strict control of a stable bed expansion at low axial mixing level [9,15,27,28]. It is crucial to achieve adsorption capacity similar to a standard chromatography in a packed-bed mode. Thus, the axial dispersion behavior of the expanded beds with the dense composite matrices was investigated to confirm whether they are suitable for expanded bed adsorption operation.

3.3.1. Effect of flow velocity and bed expansion degree

A large discrepancy between the experimental data, with regard to the dependence of axial mixing on flow velocity, has been reported. For example, Chang et al. [27] observed that the axial mixing in liquid phase using Streamline SP increased with increasing liquid velocity, while Bascoul et al. [29] described an opposite trend. Dasari et al. [30] reported that the axial mixing increased with increasing liquid velocity for 40–63-μm sized LiChroprep Si 60 silica particles but decreased for smaller sized particles (25–40 μm). In terms of the literature results, it seems that the axial mixing characteristic depends on the solid-phase type, particle size, extent of the particle size and density distributions, the column dimensions and distributor design. In this study, the axial mixing behavior in the expanded bed of the composite matrices as a function of flow velocity was examined and compared with that in the bed of Streamline SP (Fig. 5). As shown in Fig. 5a, increasing liquid velocity led to an increase of Bo from 13 to 51 for the NFBA-S. A similar result was observed for Streamline SP. For the NFBA-L, however, the Bo value was fairly constant, around 57–65, with the increase of flow velocity.

The Bo values obtained with Streamline SP in the present 9.5-mm I.D. column were between 7 and 17. These values were similar to those obtained using Streamline adsorbents in a larger diameter column (XK 16/40), as reported by Thömmes et al. [31], but lower than those obtained by other researchers (40–120) [27,32–34]. This may be due to the differences in expanded bed columns employed for the studies. Because the Bo values for the two composite matrices were higher than those for Streamline SP, it is considered that the customized adsorbents are promising for use in expanded bed operation.

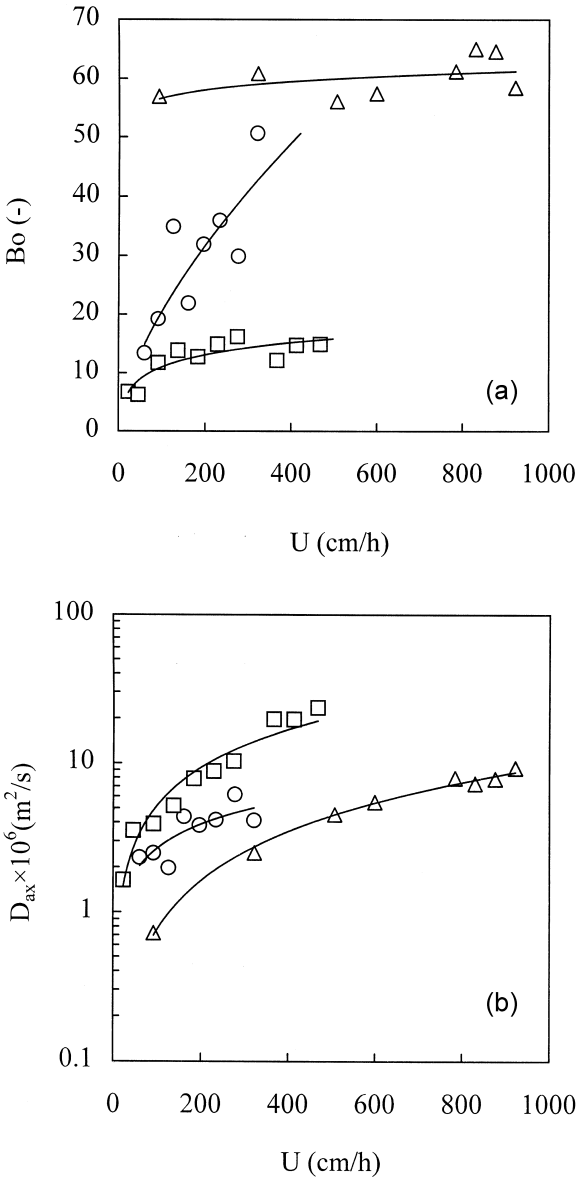

Fig. 5. Effect of flow velocity on (a) the Bodenstein number and (b) the axial mixing coefficient. Symbols and columns are the same as in Fig. 4.

Although the Bodenstein number, representing the degree of axial mixing in a column, is often used in literature [3,27,28,35], it may give a false impression of the efficiency of an expanded bed [9,33]. According to Eq. (2), the axial mixing coefficient, D_{ax}, depends on the flow velocity and the bed expansion height. Therefore, a higher Bo value may not mean a lower D_{ax}. Fig. 5b shows that the D_{ax} values of the three matrices increased with the increase of liquid velocity. The D_{ax} values in expanded bed are commonly found between 1.0×10^{-6} and 1.0×10^{-5} m^2/s at flow velocities of 100–300 cm/h [15,31]. The D_{ax} values for the NFBA-S ($2.5–4.5\times10^{-6}$ m^2/s) and NFBA-L ($0.8–2.3\times10^{-6}$ m^2/s) were in the lower limit of this range, and lower than that for Streamline SP ($5.2–12.0\times10^{-6}$ m^2/s) at flow velocities of 100–300 cm/h. In addition, the NFBA-L matrix gave the smallest D_{ax} values among the three adsorbents.

In expanded bed adsorption of proteins, the bed expansion is usually a factor 2–3. The degree of bed expansion is dependent on the liquid velocity and the size and density of the matrix. To compare three adsorbents at the same degree of bed expansion, the axial mixing coefficients of the expanded beds as a function of degree of bed expansion are provided in Fig. 6. The values for the axial mixing coefficient for the NFBA-S increased from about 3.3 to 5.1×10^{-6} m^2/s in the 2–3-fold bed expansion range, and were the smallest of the three matrices. Although the D_{ax} values for the NFBA-L were much smaller than those for Streamline SP as a function of flow velocity (Fig. 5b), their differences in the range of 2–3-fold bed expansion were not so significant. This was because of the higher flow velocity needed to reach over 2-fold bed expansion for the NFBA-L bed (Fig. 4). For the NFBA-L, only experiments at bed expansion less than 2.2 were carried out due to the upper limit in flow-rate of the piston pump (10 ml/min).

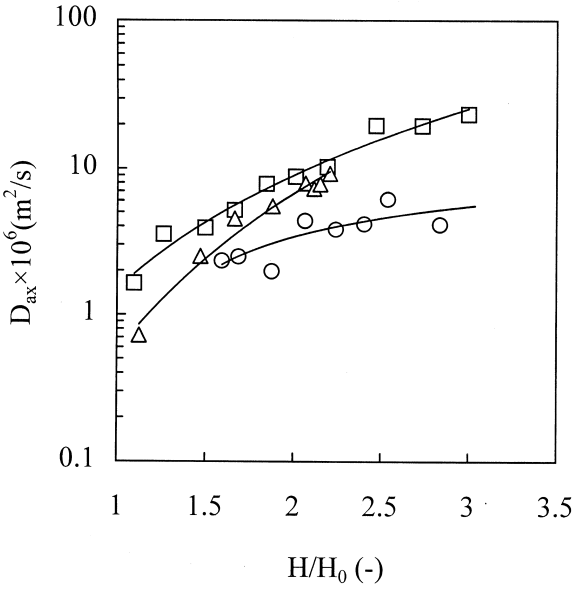

Fig. 6. Axial mixing coefficient as a function of degree of bed expansion. Symbols and columns are the same as in Fig. 4.

3.3.2. Effect of settled bed height

Fig. 7 illustrates the axial mixing behavior as a function of settled bed height. Increasing settled bed height led to an increase of Bo for the NFBA-S and NFBA-L (Fig. 7a). Such a characteristic was also observed in the experiment with Streamline SP. A similar phenomenon was observed by Thömmes et al. for the porous glass granules [35]. They accounted for this observation as the reduction of the influence of turbulence at the column inlet at a higher settled bed, which may result in flow channels at the liquid distributor.

Although a higher settled bed in an expanded bed column is required to achieve the liquid phase at a lower axial mixing level, increasing settled bed height increased the axial mixing coefficient, as shown in Fig. 7b. This is in agreement with the results reported by Lan et al. with Streamline DEAE [34]. In addition, it can been seen from Fig. 7b that the bed with the NFBA-L has the smallest axial mixing coefficient at the same settled bed height, and that with Streamline SP has the largest.

3.3.3. Effect of liquid viscosity

High-viscosity feedstocks are frequently encountered in bioseparation processes. An increase in fluid viscosity could not only decrease the liquid velocity needed to reach the same bed expansion, but also impact on the axial mixing behavior in an expanded bed. In this study, a 10% (v/v) glycerol solution (viscosity, 1.39×10^{-3} Pa s) was used to test the influence of liquid viscosity on the axial mixing. Fig.

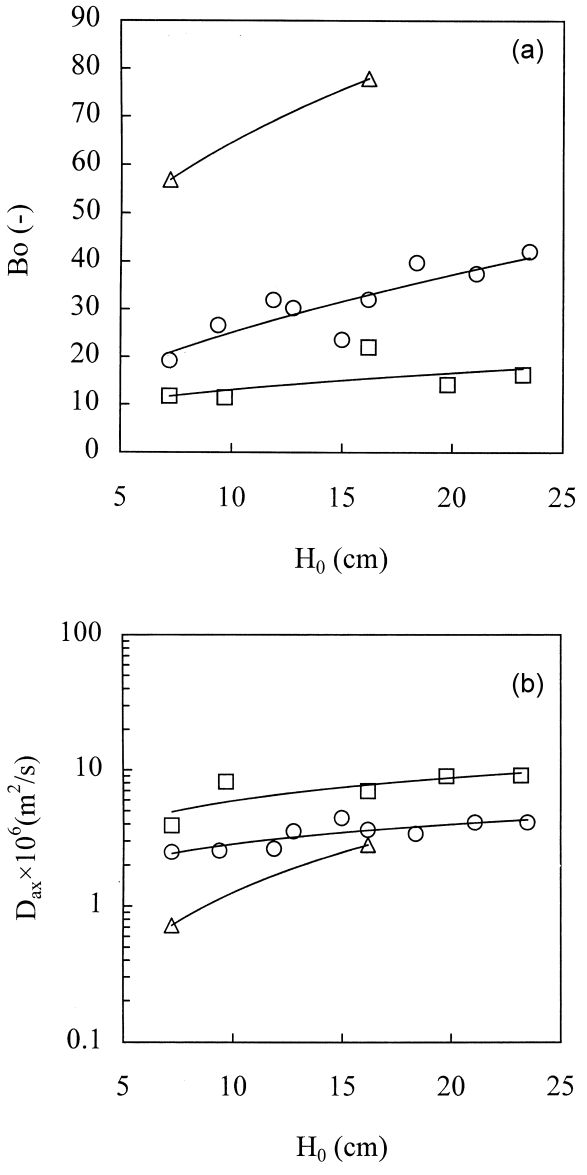

Fig. 7. Effect of settled bed height on (a) the Bodenstein number and (b) the axial mixing coefficient at a liquid superficial velocity of 92 cm/h. Symbols and columns are the same as in Fig. 4.

8 shows that increasing viscosity increased the D_{ax} values in the column. It is probably due to that the viscous liquid caused some agglomeration of the solid-phase particles, which influenced the flow behavior. A few publications have reported the viscosity effect. Chang and Chase [27] examined the influence of feedstock viscosity using Streamline SP

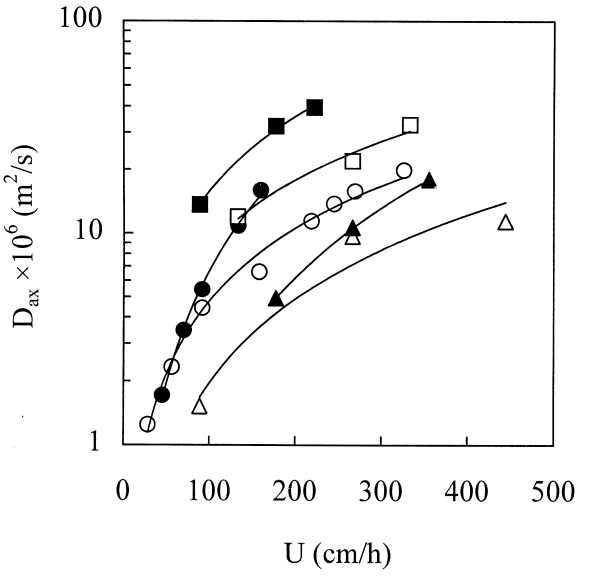

Fig. 8. Effect of liquid viscosity on bed expansion characteristics of different matrices: (○) NFBA-S/water; (●) NFBA-S/10% (v/v) glycerol; (△) NFBA-L/water; (▲) NFBA-L/10% (v/v) glycerol; (□) Streamline SP/water; (■) Streamline SP/10% (v/v) glycerol. Settled bed height was 15.0±0.2 cm.

as the solid-phase, and found that the axial mixing coefficient decreased with increasing viscosity. A similar result was observed by Pålsson et al. [9] with a customized stainless steel beads. A comparison of the D_{ax} in the beds with water and 10% (v/v) glycerol solution shows that the increase for the composite NFBA matrices was less than that for Streamline SP, especially for the NFBA-L gel. This indicates that the heavier matrix was less affected by the liquid viscosity.

3.4. Breakthrough curves

Breakthrough experiments were carried out to examine the quality of the adsorbents for expanded bed adsorption. Fig. 9 presents the results for the expanded bed adsorption of lysozyme for the CB-NFBA gels and CB-Streamline at the same velocity. It can be seen that the breakthrough curves of lysozyme for both the CB-NFBA gels were steeper than that for the CB-Streamline, indicating higher column efficiency of the expanded bed with the CB-NFBA gels at this flow velocity. This has been

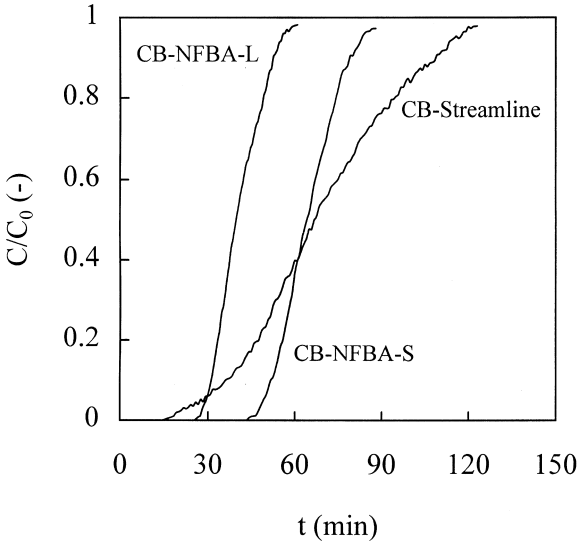

Fig. 9. Lysozyme breakthrough curves in the expanded bed of the CB-NFBA gels and CB-Streamline at 220 cm/h. Settled bed height was 5.0±0.2 cm.

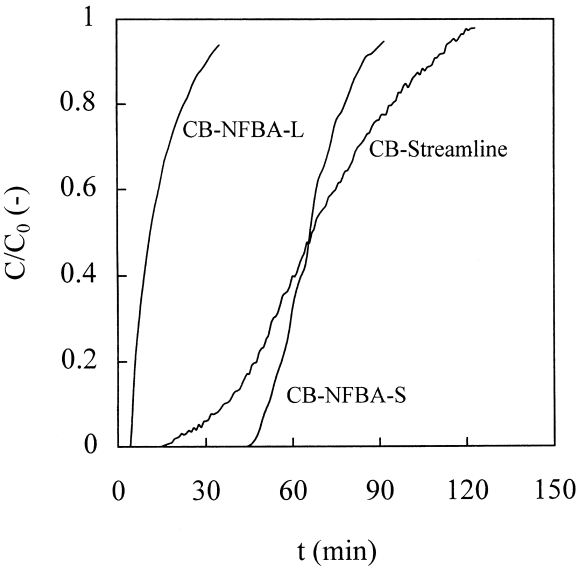

Fig. 10. Lysozyme breakthrough curves in the expanded bed of the CB-NFBA gels and CB-Streamline at 2-fold bed expansion. Settled bed height was 5.0±0.2 cm. Flow velocities were 200, 779 and 220 cm/h for CB-NFBA-S, CB-NFBA-L and CB-Streamline, respectively.

demonstrated by the results shown in Figs. 5a and 7a.

The breakthrough behavior of lysozyme in the expanded beds of the three matrices at 2-fold bed expansion but different flow velocity was then investigated and the results are shown in Fig. 10. The dynamic binding capacity (DBC) for the three adsorbents at 5% breakthrough was estimated and the results are summarized in Table 4. It can be seen from both the figure and table that the DBC for the CB-NFBA-L decreased from 16.7 to 3.7 mg/ml matrix when the superficial velocity increased from 220 to 779 cm/h. Such a phenomenon has been observed previously [12,27]. The DBC values of lysozyme for the CB-NFBA-S and CB-NFBA-L are much higher than those for CB-dyed Fractosil 1000 (5.0 mg/ml matrix) [36], but somewhat lower than those for Streamline SP [27] (50.6 mg/ml matrix). For the latter case, it may be attributed to the following two reasons. (1) The settled bed height used in this work was lower than that used by Chang and Chase [27]. The dynamic binding capacity increases with increasing settled bed height [35]. (2) The adsorption capacity of the dye–ligand adsorbents (Table 2) was smaller than that of Streamline SP [37].

The ratio of DBC to equilibrium adsorption density for each adsorbent is estimated and listed in Table 4. Here, the equilibrium adsorption density is calculated at $c = 0.5$ mg/ml from Eq. (7) with the equilibrium adsorption parameters shown in Table 2. At the same bed expansion, the ratio for the CB-NFBA-L is smaller than that for CB-Streamline. This is due to the high flow velocity needed for the NFBA-L bed. However, the ratio for the CB-NFBA-S is larger than that for CB-Streamline, in which the expanded beds were operated at nearly the same flow velocity. At the same flow velocity, the values of the ratio for the both CB-NFBA gels are larger than that for CB-Streamline. This is considered to be due to the high column efficiency for the two NFBA gels (Figs. 5a and 7a) and the small particle size of the NFBA-S gel. The results indicate that the dense composite matrices are suitable for expanded bed adsorption of proteins.

4. Conclusion

In this article, we have reported the fabrication of

Table 4
The dynamic binding capacity of lysozyme to the different matrices

Matrix	U (cm/h)	H/H_0	Bo	D_{ax} (10^{-6} m^2/s)	EAD[a] (mg/ml)	DBC[b] (mg/ml matrix)	DBC/EAD
CB-NFBA-S	200	2.0	29	2.8	66.0	23.6	0.36
	220	2.1	33	2.8		23.3	0.35
CB-NFBA-L	220	1.3	52	1.4	47.1	16.7	0.36
	779	2.0	55	5.8		3.7	0.08
CB-Streamline	220	2.0	12	7.5	59.6	12.0	0.20

[a] EAD, equilibrium adsorption density at $c=0.5$ mg/ml.
[b] DBC, dynamic binding capacity at 5% breakthrough.

Nd–Fe–B alloy-densified agarose gels for expanded bed application. The favorable properties of the NFBA gels in protein adsorption, bed expansion, axial mixing characteristics and breakthrough behavior indicate that the high-density solid assemblies are promising for application in expanded bed adsorption of protein. Since Nd–Fe–B alloy is magnetic, the composite adsorbent may also be applied to a magnetically stabilized fluidized bed (MSFB). A comparison of the MSFB with the expanded bed would give further information on the utility of the composite materials in downstream bioprocesses.

5. Symbols

Bo	Bodenstein number (–)
c	protein concentration in liquid phase (mg/ml)
c_0	initial bulk phase protein concentration (mg/ml)
d_p	particle size (μm)
D	column diameter (mm)
D_{ax}	axial mixing coefficient (m^2/s)
f	agarose gel volume fraction in the composite matrices (–)
H	expanded bed height (cm)
H_0	settled bed height (cm)
K_d	dissociation constant in the Langmuir equation (mg/ml)
q	adsorbed protein density in equilibrium with c (mg/ml)
q_m	adsorption capacity (mg/ml)
Q_d	amount of lysozyme in the dead volume (mg)
$Q_{5\%}$	amount of lysozyme adsorbed in the column at 5% breakthrough (mg)
t	time (min)
U	liquid superficial velocity (mm/s)
U_t	terminal velocity (mm/s)
V_d	dead volume (ml)
V_S	drained volume of adsorbent for expanded bed adsorption experiments (ml matrix)
ϵ	voidage of expanded bed (–)
ε_0	voidage of packed bed (–)
μ	liquid viscosity (Pa·s)
ρ	liquid density (g/ml)
ρ_A	agarose gel density (g/ml)
ρ_C	Nd–Fe–B alloy density (g/ml)
ρ_P	mean density of Nd–Fe–B alloy-densified agarose gel (g/ml)
ρ_{s_2}	solid phase density (g/ml)
σ_θ^2	variance in time unit (–)

Acknowledgements

This work was financially supported by the National Natural Science Foundation of China (grant No. 20025617).

References

[1] J. Thömmes, M. Halfar, S. Lenz, M.-R. Kula, Biotechnol. Bioeng. 45 (1995) 205.
[2] R. Hjorth, Trends Biotechnol. 15 (1997) 230.
[3] F.B. Anspach, D. Curbelo, R. Hartmann, G. Garke, W.-D. Deckwer, J. Chromatogr. A 865 (1999) 129.

[4] G.E. Hamilton, P.H. Morton, T.W. Young, A. Lyddiatt, Biotechnol. Bioeng. 64 (1999) 310.
[5] D. Lütkemeyer, N. Ameskamp, H. Tebbe, J. Wittler, J. Lehmann, Biotechnol. Bioeng. 65 (1999) 114.
[6] H.M. Fernández-Lahore, R. Kleef, M.R. Kula, J. Thömmes, Biotechnol. Bioeng. 64 (1999) 484.
[7] R.H. Clemmitt, H.A. Chase, Biotechnol. Bioeng. 67 (2000) 206.
[8] A. Pai, S. Gondkar, A. Lali, J. Chromatogr. A 867 (2000) 113.
[9] E. Pålsson, P.-E. Gustavsson, P.-O. Larsson, J. Chromatogr. A 878 (2000) 17.
[10] H.A. Chase, N.M. Draeger, J. Chromatogr. A 597 (1992) 129.
[11] G.M.S. Finette, Q.-M. Mao, M.T.W. Hearn, J. Chromatogr. A 743 (1996) 57.
[12] A. Mullick, C.M. Griffith, M.C. Flickinger, Biotechnol. Bioeng. 60 (1998) 333.
[13] C.M. Griffith, J. Morris, M. Robichaud, M.J. Annen, A.V. McCormick, M.C. Flickinger, J. Chromatogr. A 776 (1997) 179.
[14] V. Goetz, M. Remaud, D.J. Graves, Biotechnol. Bioeng. 37 (1991) 614.
[15] E. Pålsson, M.P. Nandakumar, B. Mattiasson, P.-O. Larsson, Biotechnol. Lett. 22 (2000) 245.
[16] N. Voute, D. Bataille, P. Girot, E. Boschetti, Bioseparation 8 (1999) 121.
[17] L.-Z. He, Y.-R. Gan, Y. Sun, Bioprocess Eng. 17 (1997) 301.
[18] O. Levenspiel, in: Chemical Reaction Engineering, 3rd edition, Wiley, New York, 1999.
[19] M.M. Bradford, Anal. Biochem. 74 (1976) 248.
[20] P.M. Boyer, J.T. Hsu, Chem. Eng. Sci. 47 (1992) 241.
[21] X.-D. Tong, B. Xue, Y. Sun, Biotechnol. Prog. 17 (2001) 134.
[22] B. Xue, Y. Sun, J. Chromatogr. A 921 (2001) 109.
[23] P.R. Wright, F.J. Muzzio, B.J. Glasser, Biotechnol. Prog. 14 (1998) 913.
[24] A.M. Lali, A.S. Khare, J.B. Joshi, Powder Tech. 57 (1989) 39.
[25] J.F. Richardson, W.N. Zaki, Trans. Int. Chem. Eng. 32 (1954) 35.
[26] R.B. Bird, W.E. Stewart, W.N. Lightfoot, in: Transport Phenomena, Wiley, New York, 1960.
[27] Y.K. Chang, H.A. Chase, Biotechnol. Bioeng. 49 (1996) 512.
[28] A. Karau, C. Benken, J. Thömmes, M.-R. Kula, Biotechnol. Bioeng. 55 (1997) 54.
[29] A. Bascoul, J.P. Riba, C. Alran, J.P. Couderc, Chem. Eng. J. 38 (1988) 69.
[30] G. Dasari, I. Prince, M.T.W. Hearn, J. Chromatogr. 631 (1993) 115.
[31] J. Thömmes, A. Bader, M. Halfar, A. Karau, M.-R. Kula, J. Chromatogr. A 752 (1996) 111.
[32] L.J. Bruce, S. Ghose, H.A. Chase, Bioseparation 8 (1999) 69.
[33] E. Pålsson, A. Axelsson, P.-O. Larsson, J. Chromatogr. A 912 (2001) 235.
[34] J.C.-W. Lan, G.E. Hamilton, A. Lyddiatt, Bioseparation 8 (1999) 43.
[35] J. Thömmes, M. Weiher, A. Karau, M.-R. Kula, Biotechnol. Bioeng. 48 (1995) 367.
[36] G.M.S. Finette, Q.-M. Mao, M.T.W. Hearn, Biotechnol. Bioeng. 58 (1998) 35.
[37] P.R. Wright, F.J. Muzzio, B.J. Glasser, Biotechnol. Prog. 15 (1999) 932.